2018년 2월

박사학위 논문

Regulation of Osteogenesis/Osteolysis by Induced CD133+ Prostate Cancer Cell in Bone-Marrow Microenvironmental Niches

조 선 대 학 교 대 학 원

의 학 과

김 동 휘

Regulation of Osteogenesis/Osteolysis by Induced CD133+ Prostate Cancer Cell in Bone-Marrow Microenvironmental Niches

CD133+ prostate cancer cell의 골수내 미세환경에서
골형성 및 골용해 조절에 관한 연구

2018년 2월 23일

조 선 대 학 교 대 학 원

의 학 과

김 동 휘

Regulation of Osteogenesis/Osteolysis by Induced CD133+ Prostate Cancer Cell in Bone-Marrow Microenvironmental Niches

지도교수 이 상 홍

이 논문을 의학 박사학위신청 논문으로 제출함

2017년 10월

조 선 대 학 교 대 학 원

의 학 과

김 동 휘

김동휘의 박사학위 논문을 인준함

위원장 조선대학교 교수 손 홍 문 (인)

위 원 CM충무병원 과장 이 상 훈 (인)

위 원 가톨릭대학교 교수 문 찬 웅 (인)

위 원 조선대학교 교수 임 원 봉 (인)

위 원 조선대학교 교수 이 상 홍 (인)

2017년 12월

조 선 대 학 교 대 학 원

CONTENTS

LIST OF TABLES

LIST OF FIGURES

ABSTRACT

CD133+ prostate cancer cell의 골수내 미세환경에서 골형성 및 골용해 조절에 관한 연구

김 동 휘

지도교수 : 이 상 홍

조선대학교 대학원 의학과

서론: 암 줄기세포라고 알려진 암세포 군집은 암의 전이 및 재발에 중요한 역할을 하는 것으로 알려져 있으며 특히 전립선암에서 골 전이를 촉발하는 연구가 보고되고 있다. 본 연구에서는 전립선 암세포주인 PC-3 및 DU145에서 암줄기세포의 유지를 위해 핵심 마커로 알려진 CD133 과발현시키고 이의 마우스 모델에서 골 전이 유도를 조사하고자 하였다.

실험 및 방법: 전립선 암세포주에서 CD133 과발현 세포주를 제작하고, 이를 BL-6 누드마우스의 우측 경골 골수강에 주입하였다. 골전이는 Micro-CT, 공촛점현미경, H&E 염색 그리고 면역염색화학법에 의해 분석되었다.

결과: CD133 과발현은 전립선암 세포주에서 골 전이를 유의하게 증가시켰으며 종양 경계면에서 collagen type Ⅰ, bone sialoprotein (BSP) 그리고 osteocalcin (OC)의 발현을 유의하게 증가시켰다.

결론: 종합해보면 이러한 CD133의 과발현은 전립선암의 골전이에 있어서 매우 중요한 역할을 하는 것으로 여겨진다.

색인단어: 암 줄기세포, 전립선암, 골전이, CD133, 골 형성, 골 용해

Ⅰ. INTRODUCTION

About 90% of patients with advanced prostate cancer (PC) have incurable bone metastases and a mean survival of 1 year.[1,2] Bone metastasis causes significant complications, including bone pain, impaired mobility, pathological fracture, spinal cord compression, and symptomatic hypercalcemia.[3,4] Due to the osteosclerotic nature of most bone metastases related to PC, there is a marked increase in osteoblastic activity.[5] There is, however, clear histological evidence of increased bone resorption, even in the absence of overt osteolytic bone metastases.[6,7] Therefore, a better understanding of the early mechanisms leading to the development of bone metastasis would allow therapies to be specifically targeted to lesions as they arise.

Recent identification of the critical molecular and cellular events underlying tumor progression, invasion, and metastasis to bone and other sites provides new insight into the targeting of advanced disease.[8] The hypothesis that tumors depend on a small fraction of cells, called cancer stem cells (CSCs), for long-term survival is based upon data demonstrating that subsets of human leukemic cells show tumor-initiating activity in SCID mice.[9] More recent studies suggest that CSCs are self-renewing and able to generate heterogeneous “mature” tumor progeny.[10,11] It is assumed that CSCs are typically dormant and that their “awakening” drives metastases. Primary tumors mainly comprise differentiated epithelial cells, along with a

much smaller number of cells expressing stem cell markers (i.e., PC stem-like cells).[12] In addition, a recent study shows that PC stem-like cells originating from a primary tumor have clonogenic properties and a high potential for invasion and self-renewal.[13] These cells can be identified by expression of an increasing list of CSC markers, including aldehyde dehydrogenase 1 (ALDH 1), CD133, c-Met, and prostate stem cell antigen.[14] A recent study of a cohort of high-risk PC patients revealed that the number of primary PC cells positive for the integrin subunits and the c-Met receptor correlated with bone metastasis.[15]

CD133 (also known as prominin-1) is a 5-transmembrane glycoprotein that was originally identified as a hematopoietic stem cell marker.[16] CD133 is now considered an important cell surface marker for a subpopulation of cancer-initiating cells (CICs) in brain tumors, colon carcinoma, head and neck (HN) cancer, hepatocellular carcinoma, thyroid carcinoma, and PC.[17-20] Recent reports suggest that expression of CD133 in tumor tissues is a prognostic indicator for tumor re-growth, malignant progression, and patient survival.[21] CD133 expression appears to negatively correlate with survival and prognosis of PC patients;[22] nevertheless, the mechanism by which CD133 regulates CICs during metastasis of PC to bone is unclear.

Here, we used *in vitro* and *in vivo* techniques to demonstrate that CD133 plays a crucial role in acquisition of stemness, and bone metastasis of PC cells. Considering the role of CD133 in CSC maintenance and regulation, our finding provide a plausible mechanism for bone metastasis of CSC.

II. MATERIALS AND METHODS

Chemical reagent, Cell culture and animals

All reagents were purchased from Sigma-Aldrich (St. louis. Mo). PC3 and DU145 cells were purchased from the Korean Cell Line Bank (KCLB nos. 21435 and 30081, Seoul, Korea) and maintained at 37° C in a 5% C02 humidified chamber in RPMI 1640 (Welgene, Daegu, Korea, LM 011-01) medium supplemented with 10% heat-inactivated fetal bovine serum (Gibco BRL, CA, 10082147) and 10% antibiotic-antimycotic solution (Welgene, LS203-01). After seeding, the medium was replaced with fresh medium and remaining adherent cells were allowed to reach about 70% confluence. The cells were then detached with trypsin-EDTA (Welgene, LS015-01) and re-plated with 1x104 cell/well (sub-cultured) in 6-well plates for use in experiments.

Five-week-old male athymic nude mice (BALB/C-Nu Slc; Orient Bio Co. Ltd, Seoul, Korea) were housed under standard laboratory conditions, temperature and humidity controlled cabinets, kept in 12h light-dark cycles with ad libitum access to food and water. All experimental procedures involving animals were compliant with institutional and governmental requirements and were approved by the Institutional Animal Care and Use Committee (CIACUC2015-A0032) of Chosun University, Gwangju, Korea.

Cloning of human CD133

HT29 colon cancer cells (KCLB, no. 30038) were used as a source of CD133. Cloning of CD133 was performed as described previously [23]. 293T cells were used as a positive control to check for the translated fusion product. Briefly, 293T cells were grown to near-confluence in a 60 mm dish and then transiently transfected with pcDNA3.1/NT-GFP or pcDNA3.1/NT-GFPCD133 using the FuGENE HD transfection reagent (Promega, Madison, WI, E2311) (0.2 μg of plasmid to 0.6 μL of reagent). After 48 h, the cells were gently washed with ice-cold phosphate-buffered saline (PBS).

Establishment of stably transfected PC3-GFP/DU145-GFP control cells and PC3-GFPCD133/DU145-GFPCD133 cells

Stable cell lines overexpressing GFP or the CD133-GFP fusion protein were generated by transfecting confluent PC3 or DU145 cells (in 100 mm plates) with 20 μg of pcDNA3.1/NT-GFPCD133 or pcDNA3.1/NT-GFP.[23] Briefly, cells stably expressing GFPCD133 or GFP were selected using 0.4 mg/mL G-418 sulfate (A.G. Scientific INC., San Diego, CA, G-1033) in DMEM (Welgene, LM001-05) containing 10% FBS. After transfection, surviving fluorescent cells expressing various levels of GFPCD133 or GFP were expanded in 60 mm wells. Stably transfected cells were removed using 0.05% trypsin/0.2 g/L EDTA•4Na in Hank's Balanced Salt Solution (HBSS, T&I technology, Seoul, Korea, BHB-23002) and further expanded and passaged in 100 mm tissue

culture plates in the presence of 2 mg/mL G418 to maintain expression of GFPCD133 or GFP.

Western blot analysis

When cells reached about 70% confluence, the culture medium was removed and the cells were washed twice with PBS (pH 7.4). Cell lysates were then prepared in 200 mL of cold lysis buffer (1% NP-40, 50 mM Tris-HCl, pH 7.5, 150 mM NaCl, 0.02% sodium azide, 150 mg/mL PMSF, 2 mg/mL aprotinin, 20 mg/mL leupeptin, and 1 mg/mL pepstatin A). Approximately 30 mg of tissue lysate was separated on 10% sodium dodecyl sulfate polyacrylamide gels and transferred to a polyvinylidene difluoride membrane (Amersham, Piscataway, NJ, 10600023). Each membrane was blocked with a blocking solution containing 5% skim milk in Tris-buffered saline/Tween (TBST: 2.42 g/L Tris-HCl, 8 g/L NaCl, 0.1% Tween 20, pH 7.6) for 0.5 h and then rinsed briefly in TBST. The membrane was then incubated overnight at 4° C with the following primary antibodies: anti-CD133 (1:1000; MyBioSource, San Diego, CA, MBS153507), anti-ALDHA1 (1:1000; Santa-Cruz Biotechnology, Santa-Cruz, CA, SC166362), anti-OCT-4 (1:1000; Cell Signaling Technology, Beverly, MA.#2750), anti-NANOG (1:1000, Cell Signaling Technology, #4903); or anti-DsRed2 (1:1000; Santa-Cruz Biotechnology, SC-101516). A mouse monoclonal (IgG) anti-GAPDH (1:2500; Santa-Cruz Biotechnology, SC-365062) antibody was used as a control. Finally, the membrane was washed in TBST and immunoreactivity was detected using an enhanced chemiluminescence detection kit (Merke Millipore,

Darmstadt, Germany, WBKLS0100). The intensity of the bands was determined by densitometric analysis using Image J software (http://rsb.info.nih.gov/ij).

Confocal microscopic analyses

Cells were counterstained with 4, 6-diamidino-2-phenylindole (DAPI), which was present in the ProLong Gold antifade mounting medium (Invitrogen, P36935) to visualize nuclear morphology. Digital images were captured under a TCS SP5 AOBS laser-scanning confocal microscope (Leica Microsystems, Heidelberg, Germany) fitted with a ×20 objective lens (Korea Basic Science Institute, Gwangju Center).

Colony forming assays

Non-adherent 24-well culture plates were coated with a 10% polyHEMA (Sigma,P3932) solution in absolute ethanol and dried overnight. After seeding, cells were incubated in serum-free DMEM medium supplemented with 200 ng/mL epithelial cell growth factor (R&D systems, Minneapolis, MN, 236-EG-200), 20 ng/mL basic fibroblast growth factor (Sigma-Aldrich, St. Louis, MO, SRP4038), and B-27 supplement (Invitrogen, 17504044). After 5 days of incubation, the number of spheroids in each well was counted under a light microscope (Zeiss, Zena, Germany).

Flow cytometric analysis of ALDH activity

This assay was used to examine tumor-derived cells and conducted using the ALDEFLUOR kit (StemCell Technologies, Vancouver, Canada, #01700). Cells were suspended in ALDEFLUOR assay buffer containing ALDH1 substrate (BODIPY-aminoacetaldehyde; 1 M per 106 cells) and incubated for 30 min at 37° C. Some batches of the cells were incubated with the specific ALDH1 inhibitor diethylaminobenzaldehyde (DEAB; 50 mM) and used as a negative control. Cells were then washed twice with washing buffer and analyzed by flow cytometry (FC-500, Beckman Coulter, Carlsbad, CA). Approximately 10000 counts were accumulated for each sample.

Cloning of DsRed2 protein and establishment of stably transfected PC3-DsRed2+/DU145-DsRed2+ control cells and PC3-DsRed2+GFPCD133/DU145-DsRed2+GFPCD133 cells

To examine cell distribution after injection into mice, wild-type or GFP-CD133+ PC cells were transfected with the fluorescent protein, DsRed2. Briefly, PC3/DU145 and PC3-GFPCD133/DU145-GFPCD133 cells stably expressing DsRed2 were selected using Blasticidin (10 mg/L; Invivogen, San Diego, CA, ant-bl-1) in RPMI 1640 medium containing 4 mM glutamine, 1 mM pyruvate, 4.5 g/L glucose, and 10% FBS. After transfection, surviving cells expressing various levels of DsRed2 were expanded in 60 mm culture wells. Stably transfected adherent cells were removed using 0.05% trypsin/0.2 g/L EDTA•4Na in HBSS and further expanded and passaged in 100 mm tissue culture plates in the presence of 10 mg/L Blasticidin to maintain expression of the DsRed2

protein. Images of intracellular DsRed2 and GFP expression were captured under a confocal microscope (Leica Microsystems).

Xenograft model of bone metastasis

The ability of PC cells to home to bone was examined by ex vivo imaging after intra-tibial injection into mice. The mice were anesthetized with isoflurane followed by injection of 1 × 105 PC3DsRed2+, PC3DsRed2+CD133+, DU145DsRed2+, or DU145DsRed2+CD133+ cells into the right tibia. Briefly, both knee joints were shaved and cells (in 20 μL of DMEM) were injected using a 100 μl Hamilton type syringe fitted with a 27-gauge needle. The needle was inserted into the tibia via the intercondylar fossa of the femur using a twisting motion, and cells were injected into the medullary cavity (approximately 0.3 cm proximal to the epiphy¬seal plate). To control for surgical effects, 5 μL of DMEM was injected into the contralateral limb. Following injection, 0.1 mg/kg buprenorphine was injected subcutaneously to minimize post-procedure pain and animals were returned to their cages for recovery. Ex vivo images of tumor-bearing tissues excised from mice at necropsy were obtained at 4 weeks post-injection.

Microcomputed tomography

The right femur and tibia was dissected from each mouse, and CT imaging was performed using a Quantum GX μCT imaging system (PerkinElmer, Hopkinton, MA) located at the Korea Basic Science Institute. The X-ray source was set

at 90 kV and 88 mA, with a field of view of 45 mm (voxel size, 90 μm; scanning time, 14 min). The CT images were represented in 3D Viewer, the software supplied with the Quantum GX system. Following scanning, image segmentation was performed using Analyze software (AnalyzeDirect, Overland Park, KS). Briefly, segmentation of the leg was performed using both semi-automatic and manual tools (e.g., object extraction, region growing, and objector separator) using the Volume Edit tool. Subsequently, a 3D rendering of the leg and tumor was generated and tumor volume was calculated using the ROI tool.

Histologic analysis of mouse tissues

Tissues of tumor-bearing femur and tibia were fixed in cold 4% paraformaldehyde. Bone tissue was first decalcified in a sodium citrate solution before processing and mounting on histologic slides. Decalcified femur and tibia were cut at the midpoint and embedded in paraffin blocks. Serial paraffin sections were stained with hematoxylin and eosin (H&E), and fluorescence was measured with a fluorescence microscope (Zeiss). Images of stained tissue were captured using a microscope slide scanner (3D-HISTECH Ltd., Budapest, Hungary).

Immunohistochemical analysis of bone specimens

Bone sections (3μm-thick) were deparaffinized by soaking in three changes of xylene and rehydrated in a graded series of ethanol/distilled water

solutions. For antigen retrieval, slides were placed in 0.01 M citrate-buffer (pH 6.0) and heated in a steamer for 30 min. Endogenous peroxidases were quenched by incubation in 3% hydrogen peroxide for 20 min at room temperature. Sections were incubated overnight at 4° C with the following primary antibodies (1:50 dilution): anti-collagen type 1 (Col 1; Santa-Cruz Biotechnology, sc-59772), anti-Bone sialoprotein (BSP; Santa-Cruz Biotechnology, SC-292394), anti-osteocalcin (OC; Santa-Cruz Biotechnology, SC-30045), or anti-NFATC1 (Santa-Cruz Biotechnology, SC-7294). Subsequently, sections were incubated with a biotinylated secondary antibody (LSAB; Dako Cytomation, Glostrup, Denmark, K0675) for 30 min, washed in PBS, and incubated with a streptavidin-peroxidase conjugate (LSAB, Dako Cytomation, K0609) for 30 min. The reaction was developed using 3, 30-diaminobenzidine tetrahydrochloride (Sigma-Aldrich, S-1141) for 5 min. Slides were briefly counterstained in hematoxylin, dehydrated, and cover slipped. Negative and positive controls were run simultaneously. Mammary tissue served as a positive control. Images were captured using a microscope slide scanner (3D-HISTECH Ltd).

Enzyme-linked immunosorbent assay

Receptor activator of nuclear factor κB ligand (RANKL) levels in cell supernatants and serum from xenograft model mice were measured using a commercially available enzyme immunoassay kit (R&D Systems, MTR00), according to the manufacturer's protocol. Absorbance was measured in a

colorimetric microplate reader (Biotek, Winooski, VT) at 450 nm. The reading was then subtracted from the reading at 570 nm.

Statistical analysis

A two-tailed, paired Student t test was used for statistical analyses, and P values < 0.05 were considered statistically significant. Data are expressed as the mean ± standard deviation (SD) unless otherwise specified. GraphPad Prism (version 6.00) software for Windows (GraphPad, La Jolla, CA) was used to analyze data from the animal model and all other data were analyzed using SPSS version 20.0 for Windows (SPSS, Chicago, IL).

III. RESULTS

Stable overexpression of CD133 and Stem cell-like properties in PC3 and DU145 cells

To determine the effect of CD133 overexpression in vitro, we first established cell lines stably overexpressing CD133 under the control of a constitutive promoter. Specifically, PC3 and DU145 cells were transfected with either GFP-tagged CD133 or empty vector containing GFP alone. A representative CD133GFP clone was then selected from each line (PC3CD133+ and DU145CD133+) and compared with the corresponding control cell line transfected with GFP alone (PC3Vec and DU145Vec). 293T cells transiently transfected with GFP (293TVec) or CD133GFP (293TCD133+) were used as a positive control. PC3Vec and DU145Vec showed very low basal expression of CD133; however, expression was significantly higher in PC3CD133+ and DU145CD133+ and in transiently transfected 293T cells(Fig. 1). PC3CD133+ and DU145CD133+ expressed green fluorescence in both the cytosol and cell membrane(Fig. 2).

To examine the role of CD133 in cancer “stemness”, we analyzed the cells for CSC-like properties (e.g., increased ability to form tumor spheres, ALDH activity, and expression of stem cell-like markers such as ALDHA1, OCT4, and NANOG). PC3CD133+ and DU145CD133 showed increased expression of OCT4, ALDHA1, and NANOG, consistent with increased stemness(Fig. 3). Stemness was also confirmed by the colony formation assay. PC3CD133+ and DU145CD133+

cells were significantly better able to form colonies than control cells, which is again concordant with increased stemness(Fig. 4).

We then used the ALDEFLUOR assay to examine PC3CD133+ and DU145CD133+ cells showing ALDH activity(Fig. 5). We found that 1.5% and 3.4% of PC3Vec and DU145Vec cells, respectively, were ALDEFLUOR-positive. By contrast, 5.5% and 4.6% of PC3CD133+ and DU145CD133+ cells, respectively, were ALDEFLUOR-positive. These results demonstrate that ectopic overexpression of CD133 by PC cells increased ALDH activity, colony forming ability, and expression of ALDHA1, OCT4, and NANOG.

Stable overexpression of DsRed2 in PC3 and DU145 cells and CD133 promotes PC3/DU145-induced osteolytic bone fracture in vivo

To monitor the distribution of cells injected into the mouse metastatic xenograft model, PC3wild/PC3GFPCD133+ and DU145wild/DU145GFPCD133+ cells were transfected with DsRed2. Expression of DsRed2 was significantly higher in PC3DsRed2+/PC3DsRed2+GFPCD133+ and DU145DsRed2+/DU145DsRed2+GFPCD133+ cells than in control cells(Fig. 6). Also, PC3DsRed2+/PC3DsRed2+GFPCD133+ and DU145DsRed2+/DU145DsRed2+GFPCD133+ cells expressed red fluorescence in both the cytosol and cell membrane(Fig. 7). Therefore, mice were injected with PC3DsRed2+GFPCD133+/DU145DsRed2+GFPCD133+ or PC3DsRed2+/DU145DsRed2+ (control) cells (see below).

In addition, we asked how PC cells formed tumors by injecting PC3DsRed2+GFPCD133+/DU145DsRed2+GFPCD133+ or PC3DsRed2+/DU145DsRed2+ cells

into the tibia of mice and then examining bone tumor growth. The PC3DsRed2+GFPCD133+ skeletal tumors clearly caused osteolytic bone fracture, as shown in the 3D micro-CT scanning images from tumor-bearing mice compared with those from PC3DsRed2+ mice(Fig. 8). Relative bone volume in the left tibia was significantly lower (0.68) following injection of PC3DsRed2+GFPCD133+ than after injection of PC3DsRed2(Fig. 9). The volume of bone tumors in the tibia of PC3DsRed2+GFPCD133+-inoculated mice was higher than that in control mice (up to 200 mm3 vs. 25 mm3, respectively)(Fig. 10). By contrast, the tumor volume in DU145DsRed2+GFPCD133+ mice was only 18 mm3.

The table 1 shows that only 30% of PC3DsRed2+-inoculated animals developed skeletal tumors (n = 10) compared with 100% of PC3DsRed2+GFPCD133+-inoculated animals. However, 40% of DU145DsRed2+GFPCD133+-inoculated mice developed tibial tumors compared with none of the DU145DsRed2+-inoculated mice. Taken together, these data suggest that ectopic overexpression of CD133 significantly increases the formation of bone tumors in vivo; thus it is possible that increased CD133 expression increases the risk of metastasis.

Histologic findings and distribution of CD133-overexpressing PC3/DU145 cells

Intra-tibial inoculation of cancer cells is commonly used to establish an experimental model of bone metastasis. To examine the histologic features of the skeletal tumors induced by inoculation of PC3DsRed2+/PC3DsRed2+GFPCD133+ or DU145DsRed2+/DU145DsRed2+GFPCD133+ cells, we performed H&E staining of bone sections. As shown in Figure 11, gross necropsy revealed that the tumor

mass in the tibia generally occupied the primary spongiosum (trabecular epiphysis) region and displaced the bone marrow cells. Notably, this was not the case for DU145DsRed2+ cells, where there was an apparent margin between the bone and the tumor. However, osteogenic or osteolytic features were present in tibia inoculated with PC3DsRed2+GFPCD133+ or DU145DsRed2+GFPCD133+.

To investigate the distribution of inoculated PC cells in the tibia, we examined GFP and DsRed2 fluorescence. Figure 12 shows that a strong GFP fluorescence signal was detected near the tumor and bone interface, and a weak signal was detected in the region of the tumor mass, in tibias injected with PC3DsRed2+GFPCD133+ or DU145DsRed2+GFPCD133+ cells. This suggests that CD133-overexpressing cells attached to and interacted with bone cells to induce osteogenic/osteolytic activity.

Expression of osteogenic/osteolytic protein and molecular events associated with osteolytic features

Although clinically identified PC bone metastases show a predominant osteoblastic phenotype (with some osteolytic features), inoculation of PC cells induced mainly osteolytic bone fractures. Therefore, to assess whether overexpression of CD133 affects the osteogenic/osteolytic phenotype of PC3/DU145 cells, we evaluated expression of Col 1, BSP, OC, and NFATC1 by PC3DsRed2+/PC3DsRed2+GFPCD133+ and DU145DsRed2+/DU145DsRed2+GFPCD133+ cells in the mouse tibia. As shown in Figure 13, positive expression of Col 1, OC,

and NFATC1 was observed in the trabecular epiphysis region in tibias injected with PC3DsRed2+GFPCD133+ or DU145DsRed2+GFPCD133+. In addition, slight BSP expression was detected in the trabecular epiphysis region in tibias inoculated with PC3DsRed2+GFPCD133+. These observations suggest that ectopic overexpression of CD133 leads to both osteogenic and osteolytic activity in the bone area adjacent to the tumor.

Finally, to assess the osteolytic activity of PC cell lines, we measured the amount of RANKL released into the cell culture supernatants and into the bloodstream of mice injected with PC3DsRed2+/PC3DsRed2+GFPCD133+ or DU145DsRed2+/DU145DsRed2+GFPCD133+ cells(Fig. 14, 15). In all cases, PC3DsRed2+GFPCD133+ and DU145DsRed2+GFPCD133+ cells induced greater release of RANKL than control cells. This observation strongly suggests that CD133 overexpression in PC contributes to systemic osteolytic bone fracture and bone metastasis.

IV. Discussion

Bone is a common and important site of distant PC metastasis[24]. Despite advances in our understanding of the mechanisms underlying the basic molecular biology of bone metastasis, there is currently no curative treatment for metastatic disease; thus bone metastasis remains a devastating complication of advanced PC. Recent research suggests that CSCs play a pivotal role in PC metastasis. CSCs are a small cell population that is responsible for the initiation and maintenance of tumor burden and therapeutic refractoriness.[25] Acquisition of the capacity for self-renewal and stemness is essential for tumorigenesis and for continued accumulation of oncogenic changes that lead to cancer.[26] Here, we first sought to identify CSC-like cells by inducing ectopic overexpression of CD133 in two PC cancer cell lines: PC3 and DU145. Overexpression induced genetic changes in PC cells leading to expression of several factors related to stemness, including OCT4, ALDHA1, and NANOG, which endowed cells with colony forming ability and ALDH activity. CD133-expressing cancer cells with stem cell-like phenotypes play a role in tumor recurrence.[27] CD133 is also thought to be a common marker for stemness; it is expressed by normal tissue-resident and hematopoietic stem cells but is no longer detectable following differentiation. Likewise, cancer cells stop expressing CD133 upon differentiation.[28] Colon, lung, and hematopoietic CSCs are isolated by cell sorting according to expression of CD133, though the function of CD133

remains unclear.[29] CD133-expressing cells grow indefinitely in vitro and form spheres; they also show tumorigenicity in vivo. Here, we found that overexpression of CD133 endowed PC cells with stem-like properties. In this study, we demonstrate for the first time that PC cells can acquire stem cell-like properties upon ectopic overexpression of CD133.

The following question then arises: is it possible that PC cells can acquire CSC-like properties, which triggers formation of bone metastases? To answer this, we transfected PC cells with CD133 plus GFP and DsRed2 and then injected them into the tibias of athymic nu/mice. Considering that CSCs can give rise to both CSCs and non-CSCs (i.e., the process is reversible), we expected that CD133+ cells would also give rise to CD133+ and CD133- cells. Hongo et al. reported that CD133+ cells can give rise to CD133- cells but not vice versa, suggesting that CD133 is responsible for stemness.[30] CSCs expand their colonies through asymmetric cell division, resulting in two daughter cell populations: one is similar to the mother cell (thereby retaining stem cell properties) while the other is committed to undergo differentiation into a specific lineage.[31] These characteristics of CSCs are responsible for tumor heterogeneity, meaning that CD133 expression can vary widely within a cancer cell line or within a single tumor.[32] Therefore, to induce the bias of tumor heterogeneity, we changes of bone. The findings indicated that CD133 is likely one of several stem cell-related molecules involved in the metastasis of PC cells to bone. Specifically, expression of CD133 by PC3 and DU145 cells leads to metastasis to the tibia and subsequent

osteolytic bone fracture after injection into mice. CT and histological findings revealed that CD133+ cells generated larger and more aggressive tumors than control cells. Also, inoculation of CD133+ prostate designed CD133-transfection in a single cell line of PC and then comparatively analyzed the biologic characteristics of CD133+ and wild type. In the present study, PC3DsRed2+GFPCD133+ and DU145DsRed2+GFPCD133+ cells expressed both GFP and DsReD2 and generated a tumor mass in the tibia; moreover, the GFP signal was the most intense at the interface between bone and tumor. Thus, CD133+ cells showing stemness may attach directly to bone, resulting in a higher rate of bone fracture and osteolysis. Detailed histomorphometric analyses revealed that the fast-growing intra-tibial tumors caused heterogeneous lesions, accompanied by increased lysis and sclerosis, when compared with control tumors at the same time points.

The most apparent feature of the PC3DsRed2+GFPCD133+/DU145DsRed2+GFPCD133+ intra-tibial tumors was markedly increased damage to the local bone structure. For example, micro-CT and histologic analyses revealed that PC3DsRed2+GFPCD133+ tumors almost completely destroyed the tibial bone architecture at 4 weeks post-inoculation; however, PC3DsRed2+ tumors caused much less severe damage. Immunostaining for NFATC1 revealed a high number of osteoclasts at the intra-tibial tumor/bone interface, which corresponded with large amounts of RANKL in the cell supernatant and serum; these findings may account for the massive and localized net bone lysis observed after injection of PC3DsRed2+GFPCD133+. NFATC1 is osteoclastic markers

expressed by highly active osteoclasts and RANKL is necessary for osteoclast formation and activity for bone lysis from its committed precursors with its receptor RANK.[24)]

As previously described, CD133+ PC3 cells show a predominantly lytic response in the bone, although deposition of new bone also occurs.[24)] Similarly, clinical studies show that, in most PC patients, lesions in metastatic foci are accompanied by both bone destruction and bone formation [33-35)]. The tropism of PC cells for bone suggests that they may preferentially interact with specific cells in the bone microenvironment: the most likely candidates are osteoblasts.[36)] Radiologic and histomorphometric evidence indicates that sites of PC bone metastases often show microscopic evidence of increased bone production, including increased osteoid surface area, volume, and mineralization rate.[4)] These histological findings are consistent with our findings of increased expression of osteogenic markers such as Col 1, BSP and especially, OC in PC3DsRed2+GFPCD133+- or DU145DsRed2+GFPCD133+- inoculated tibiae. However, increased RANKL concentration in the cell supernatant and serum suggests osteoclast activity, which in turn suggests that PC induces bone production through an overall increase in bone remodeling. In the case of PC, it appears that induction of osteoblast-mediated mineralization eventually outweighs the increase in osteoclast-mediated resorption, resulting in the net formation of osteoblastic lesions.[24)]

CD133 may be a candidate biomarker for bone metastasis in PC patients. The inability to predict which patients will develop metastatic disease remains a major challenge to PC management and results in unnecessary treatment for some and delayed or insufficient treatment for others.[36] Although the presence of circulating PC cells in the blood is an indication that tumor cells have disseminated from the primary site, the association between circulating tumor cells and bone metastasis remains controversial. It may be that only a subset of circulating tumor cells possesses the necessary properties to target bone.

V. Conclusion

In light of the significant advances in research into stem cells and metastasis, we propose that bone metastasis of PC occurs according to the CSC-based model. Taken together, our findings indicate that CD133 plays a functional role in regulating the stem cell-like properties of PC cells, leading to sustained acquisition of both osteolytic and osteogenic features. These data also support a role for stem cells in PC metastasis to bone. Therefore, these results should facilitate development of a novel classification system and therapeutic strategies for bone metastasis.

REFERENCES

1. Bubendorf L, Schopfer A, Wagner U, et al. Metastatic patterns of prostate cancer: an autopsy study of 1,589 patients. Hum Pathol. 2000;31:578-83.
2. Rana A, Chisholm GD, Khan M, Sekharjit SS, Merrick MV, Elton RA. Patterns of bone metastasis and their prognostic significance in patients with carcinoma of the prostate. Br J Urol. 1993;72:933-6.
3. Galasko CS. Skeletal metastases. Clin Orthop Relat Res. 1986:18-30.
4. Keller ET, Brown J. Prostate cancer bone metastases promote both osteolytic and osteoblastic activity. J Cell Biochem. 2004;91:718-29.
5. Pecherstorfer M, Zimmer-Roth I, Schilling T, et al. The diagnostic value of urinary pyridinium cross-links of collagen, serum total alkaline phosphatase, and urinary calcium excretion in neoplastic bone disease. J Clin Endocrinol Metab. 1995;80:97-103.
6. Charhon SA, Chapuy MC, Delvin EE, Valentin-Opran A, Edouard CM, Meunier PJ. Histomorphometric analysis of sclerotic bone metastases from prostatic carcinoma special reference to osteomalacia. Cancer. 1983;51:918-24.
7. Clarke NW, McClure J, George NJ. Morphometric evidence for bone resorption and replacement in prostate cancer. Br J Urol. 1991;68:74-80.
8. Nakazawa M, Kyprianou N. Epithelial-mesenchymal-transition regulators in prostate cancer: Androgens and beyond. J Steroid Biochem Mol Biol. 2016;
9. Lapidot T, Sirard C, Vormoor J, et al. A cell initiating human acute myeloid leukaemia after transplantation into SCID mice. Nature. 1994;367:645-8.
10. Al-Hajj M, Wicha MS, Benito-Hernandez A, Morrison SJ, Clarke MF. Prospective

identification of tumorigenic breast cancer cells. Proc Natl Acad Sci U S A. 2003;100:3983-8.

11. Sampieri K, Fodde R. Cancer stem cells and metastasis. Semin Cancer Biol. 2012;22:187-93.
12. Klonisch T, Wiechec E, Hombach-Klonisch S, et al. Cancer stem cell markers in common cancers - therapeutic implications. Trends Mol Med. 2008;14:450-60.
13. Yu C, Yao Z, Jiang Y, Keller ET. Prostate cancer stem cell biology. Minerva Urol Nefrol. 2012;64:19-33.
14. Kryczek I, Liu S, Roh M, et al. Expression of aldehyde dehydrogenase and CD133 defines ovarian cancer stem cells. Int J Cancer. 2012;130:29-39.
15. Colombel M, Eaton CL, Hamdy F, et al. Increased expression of putative cancer stem cell markers in primary prostate cancer is associated with progression of bone metastases. Prostate. 2012;72:713-20.
16. Shmelkov SV, St Clair R, Lyden D, Rafii S. AC133/CD133/Prominin-1. Int J Biochem Cell Biol. 2005;37:715-9.
17. Major AG, Pitty LP, Farah CS. Cancer stem cell markers in head and neck squamous cell carcinoma. Stem Cells Int. 2013;2013:319489.
18. Singh SK, Hawkins C, Clarke ID, et al. Identification of human brain tumour initiating cells. Nature. 2004;432:396-401.
19. Ricci-Vitiani L, Pagliuca A, Palio E, Zeuner A, De Maria R. Colon cancer stem cells. Gut. 2008;57:538-48.
20. Collins AT, Berry PA, Hyde C, Stower MJ, Maitland NJ. Prospective identification of tumorigenic prostate cancer stem cells. Cancer Res. 2005;65:10946-51.
21. Li T, Su Y, Mei Y, et al. ALDH1A1 is a marker for malignant prostate stem

cells and predictor of prostate cancer patients' outcome. Lab Invest. 2010;90:234-44.

22. Hurt EM, Kawasaki BT, Klarmann GJ, Thomas SB, Farrar WL. CD44+ CD24(-) prostate cells are early cancer progenitor/stem cells that provide a model for patients with poor prognosis. Br J Cancer. 2008;98:756-65.
23. Moon Y, Kim D, Sohn H, Lim W. Effect of CD133 overexpression on the epithelial-to-mesenchymal transition in oral cancer cell lines. Clin Exp Metastasis. 2016;33:487-96.
24. Valta MP, Tuomela J, Bjartell A, Valve E, Vaananen HK, Harkonen P. FGF-8 is involved in bone metastasis of prostate cancer. Int J Cancer. 2008;123:22-31.
25. Lee KH, Ahn EJ, Oh SJ, et al. KITENIN promotes glioma invasiveness and progression, associated with the induction of EMT and stemness markers. Oncotarget. 2015;6:3240-53.
26. Li F, Tiede B, Massague J, Kang Y. Beyond tumorigenesis: cancer stem cells in metastasis. Cell Res. 2007;17:3-14.
27. Uchida N, Buck DW, He D, et al. Direct isolation of human central nervous system stem cells. Proc Natl Acad Sci U S A. 2000;97:14720-5.
28. Mizrak D, Brittan M, Alison M. CD133: molecule of the moment. J Pathol. 2008;214:3-9.
29. Yu CC, Hu FW, Yu CH, Chou MY. Targeting CD133 in the enhancement of chemosensitivity in oral squamous cell carcinoma-derived side population cancer stem cells. Head Neck. 2016;38 Suppl 1:E231-8.
30. Hongo K, Tanaka J, Tsuno NH, et al. CD133(-) cells, derived from a single human colon cancer cell line, are more resistant to 5-fluorouracil (FU) than CD133(+) cells, dependent on the beta1-integrin signaling. J Surg Res.

2012;175:278-88.

31. Lee MR, Ji SY, Mia-Jan K, Cho MY. Chemoresistance of CD133(+) colon cancer may be related with increased survivin expression. Biochem Biophys Res Commun. 2015;463:229-34.

32. Diaz-Cano SJ. Tumor heterogeneity: mechanisms and bases for a reliable application of molecular marker design. Int J Mol Sci. 2012;13:1951-2011.

33. Roudier MP, Vesselle H, True LD, et al. Bone histology at autopsy and matched bone scintigraphy findings in patients with hormone refractory prostate cancer: the effect of bisphosphonate therapy on bone scintigraphy results. Clin Exp Metastasis. 2003;20:171-80.

34. Maeda H, Koizumi M, Yoshimura K, Yamauchi T, Kawai T, Ogata E. Correlation between bone metabolic markers and bone scan in prostatic cancer. J Urol. 1997;157:539-43.

35. Demers LM, Costa L, Lipton A. Biochemical markers and skeletal metastases. Cancer. 2000;88:2919-26.

36. Chu K, Cheng CJ, Ye X, et al. Cadherin-11 promotes the metastasis of prostate cancer cells to bone. Molecular cancer research : MCR. 2008;6:1259-67.

Table 1. Characteristics of the intra-tibial tumors. *P* values (Chi squared test) were used to compare tumor occurrence or invasion after injection of $PC3^{DsRed2+CD133+}$ or $PC3^{DsRed2+}$, or $DU145^{DsRed2+CD133+}$ or $DU145^{DsRed2}$, cells

Cell lines	$PC3^{DsRed2+}$	$PC3^{D/sRed2+GFPCD133+}$	$DU145^{DsRed2+}$	$DU145^{DsRed2+GFPCD133+}$
Tumor occurrence % (Number of mice with tumors/mice in study)	3/10 (30%)	10/10 (100%), P<0.05	0/10 (0%)	4/10 (40%)
Tumor invasion outside bone marrow cavity % (Number of mice with invading tumor/mice in study)	2/10 (20%)	10/10 (100%), P<0.05	0/10 (0%)	2/10 (20%)

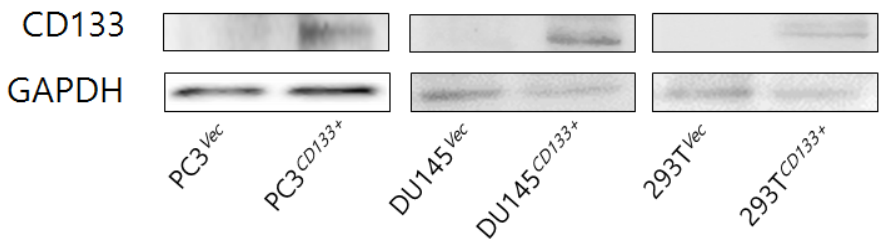

Figure 1. Western blot analysis of CD133 expression in PC3vec/DU145vec (controls) and PC3CD133+/DU145CD133+ (CD133-overexpressing) cells. 293T cells were transiently transfected with pcDNA3.1/NT-GFP or pcDNA3.1/NT-GFPCD133 as negative/positive controls.

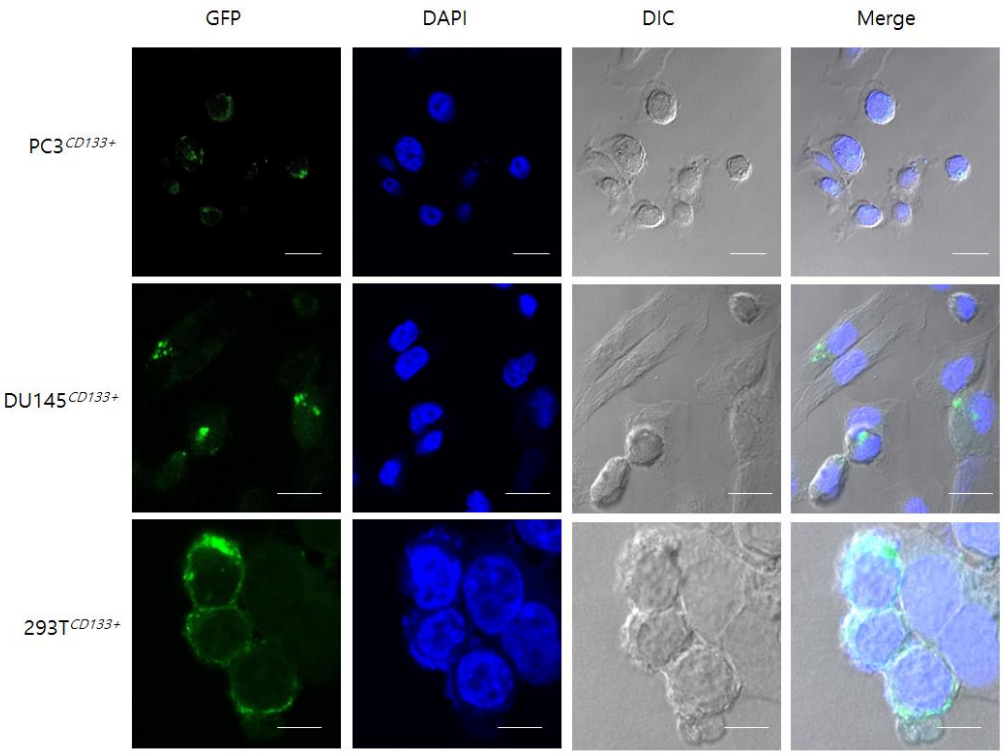

Figure 2. Confocal microscopy analysis of GFPCD133 expression in stably or transiently transfected PC3/DU145/293TGFPCD133+ cells. Nuclei were stained with DAPI (blue). Images were taken at 630× magnification. Bar, 10 μm.

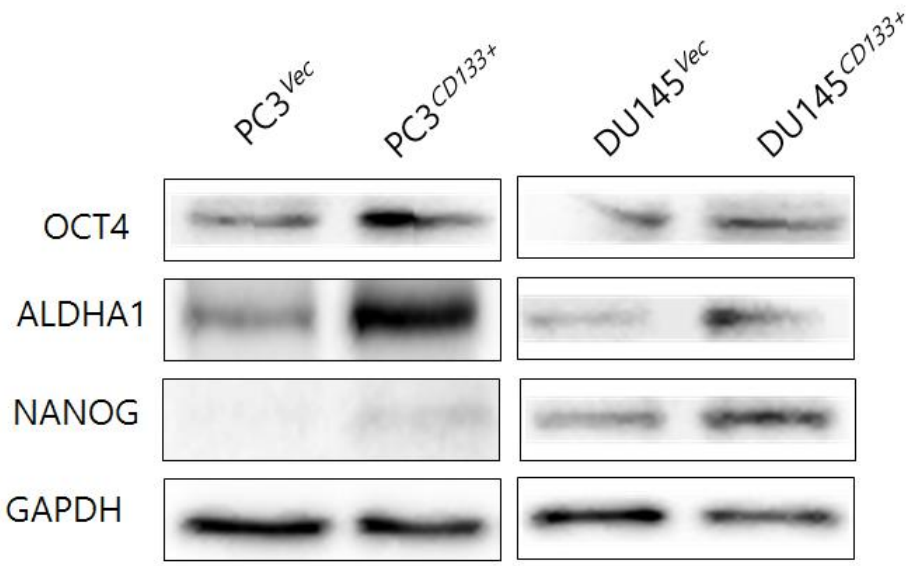

Figure 3. Expression of stemness-related proteins was characterized by western blotting. GAPDH was used as a loading control. Results are representative of three separate experiments, all with similar results.

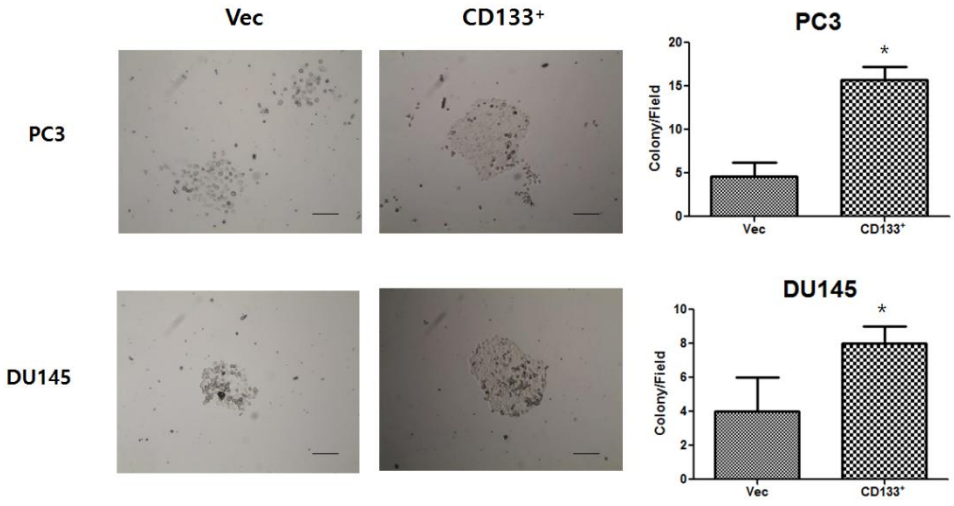

Figure 4. Stable overexpression of CD133 led to a significant increase in the ability of PC3 and DU145 cells to form colonies. Images were taken at 100× magnification. Bar, 100 μm. Data in the bar graphs are expressed as the mean ± standard deviation (SD). *, $P < 0.05$.

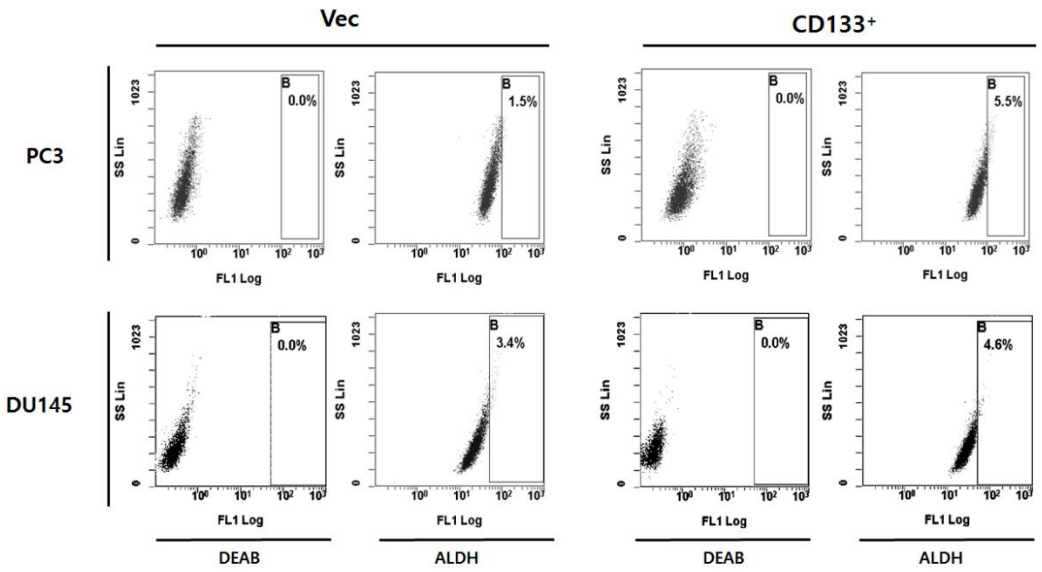

Figure 5. Representative flow cytometry plots showing ALDH activity in prostate cancer cells. In each case (Vec or CD133+ cells) the plots on the left show negative controls cells treated with the ALDH inhibitor, diethylaminobenzaldehyde. The gated cell populations (labeled B) represent the ALDH-positive subpopulations.

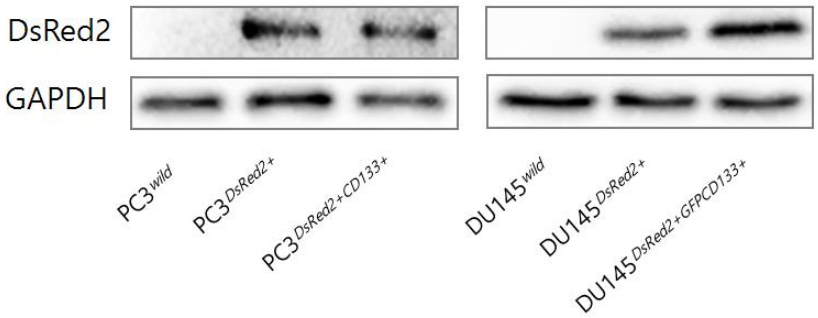

Figure 6. Western blot analysis of DsRed2 expression in PC3wild/PC3DsRed2+/PC3DsRed2+CD133+ and DU145wild/DU145DsRed2+/DU145DsRed2+CD133+ cells.

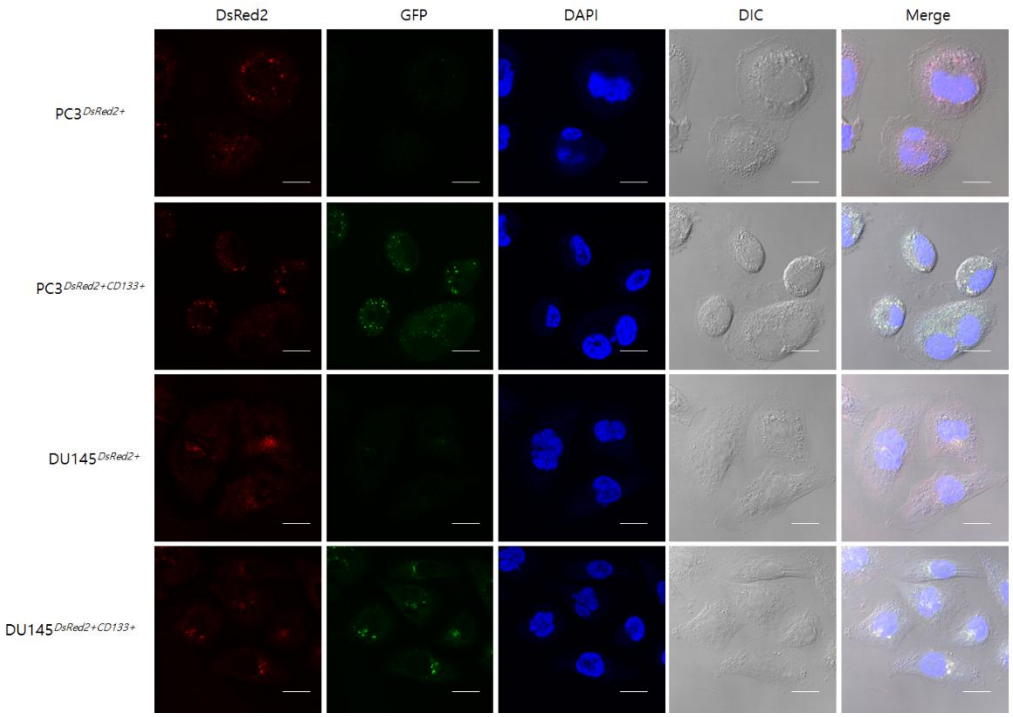

Figure 7. Confocal microscopy analysis of DsRed2 expression in stably transfected PC3DsRed2+/PC3DsRed2+CD133+ and DU145DsRed2+/DU145DsRed2+CD133+ cells. Nuclei were stained with DAPI (blue). Images were taken at 630× magnification. Bar, 10 μm.

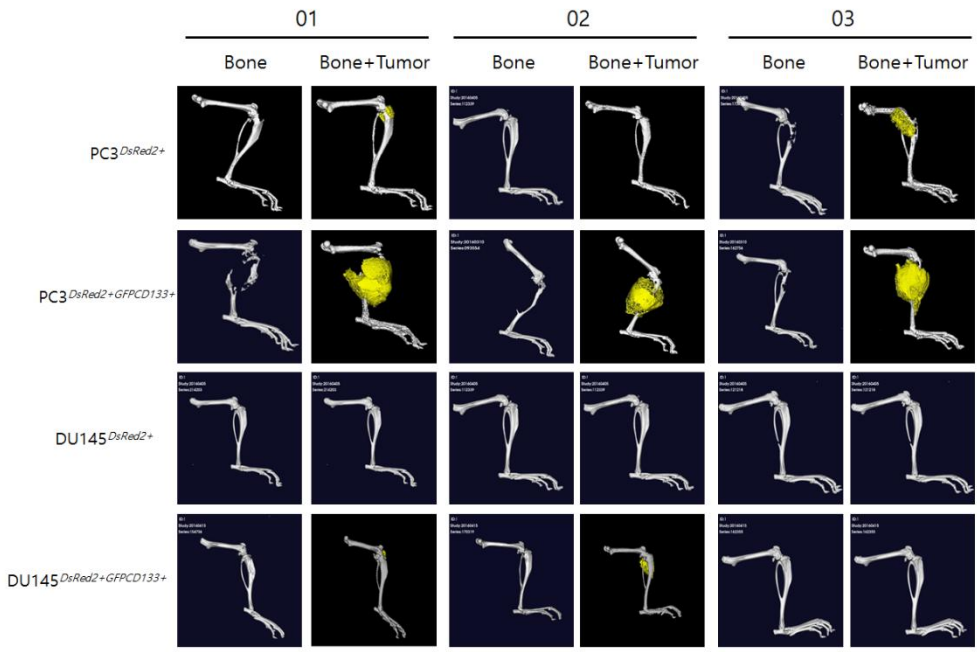

Figure 8. Representative microcomputed tomography (μCT) images of tibias in mice at 28 days post-injection of PC3DsRed2+/PC3DsRed2+CD133+ or DU145DsRed2+/DU145DsRed2+CD133+ cells. Entire tibiae (Bone) were imaged using μCT, and reconstructed 3-dimensional images were used to visually assess bone tumors (Bone+Tumor).

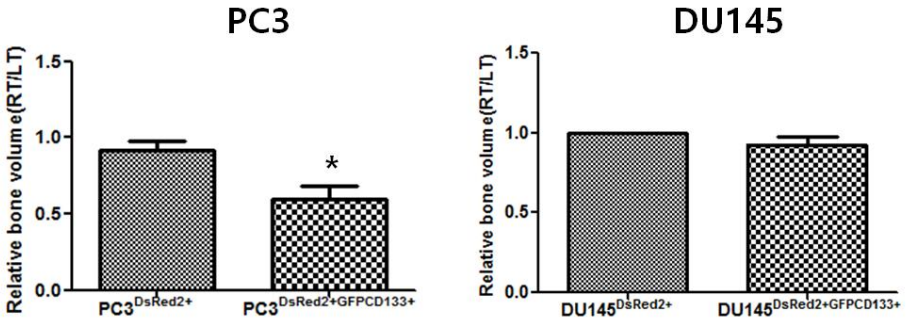

Figure 9. To measure bone destruction, the bone content of the tumor-bearing right (RT) and non-tumor-bearing left (LT) tibiae was measured and compared. n = 10. * P < 0.05.

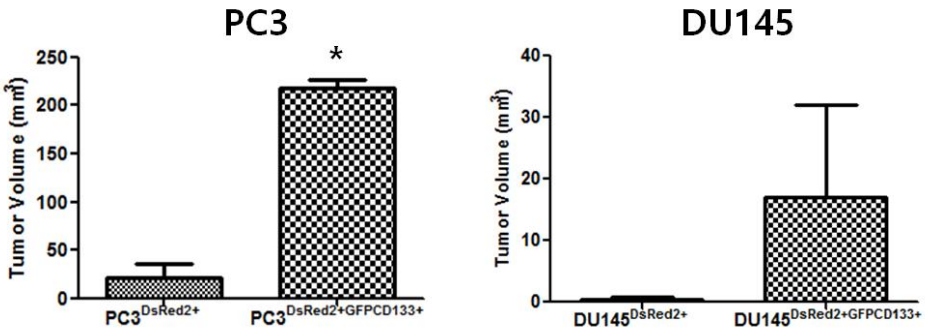

Figure 10. Tumor volume was calculated using the ROI tool after 3D rendering of the leg. Volume is expressed as the mean ± SD.

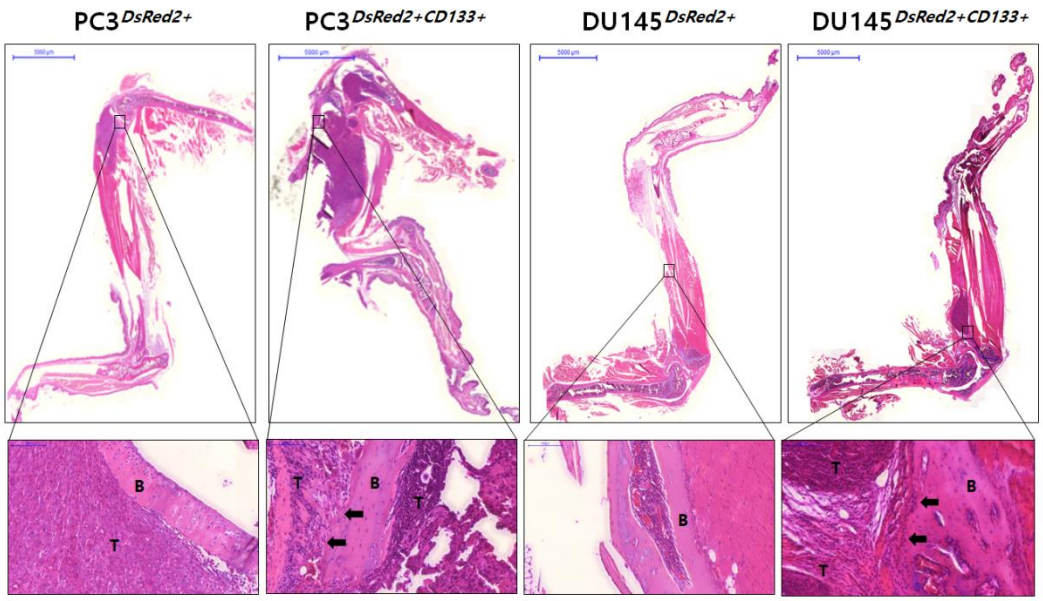

Figure 11. Sections of mouse tibiae were stained with hematoxylin and eosin (H&E) after inoculation of PC3DsRed2+/PC3DsRed2+CD133+ or DU145DsRed2+/DU145DsRed2+CD133+ cells and examined at low (upper panel; 10×; Bar, 5000 μm) and high (lower panel; 200×; Bar, 100 μm) magnification. B; Bone, T; Tumor mass.

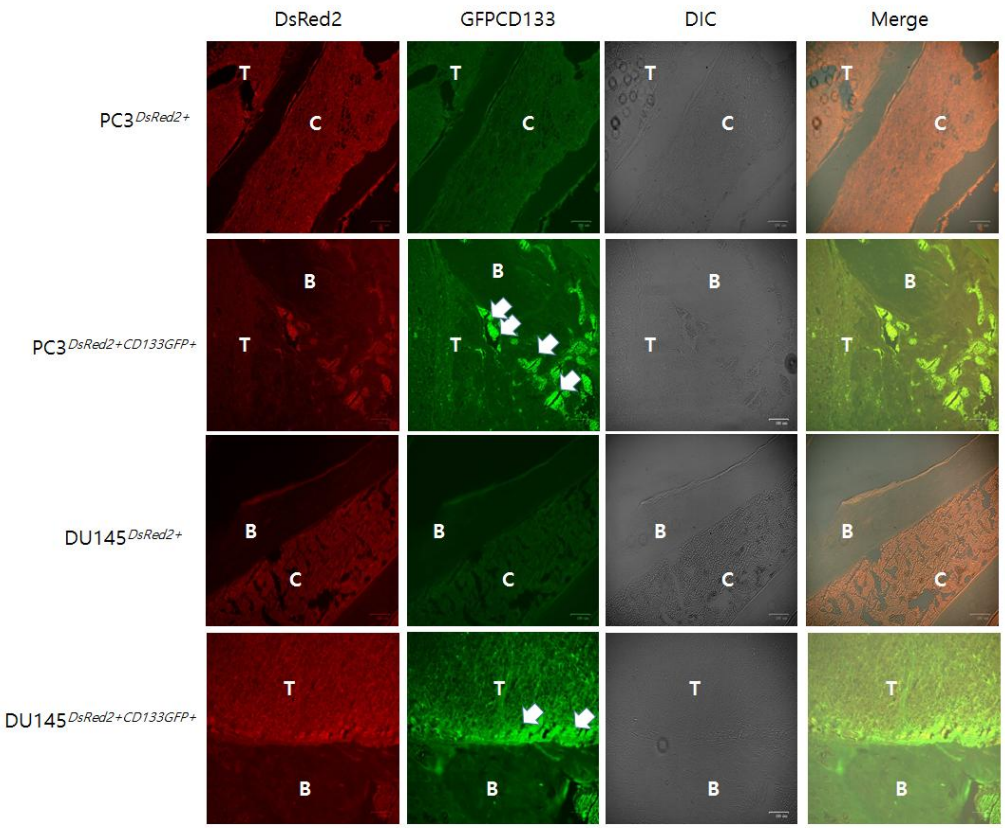

Figure 12. Immunofluorescence analysis of GFP and DsRed2 expression in the tibiae of mice at 28 days post-injection of PC3DsRed2+/PC3DsRed2+CD133+ or DU145DsRed2+/DU145DsRed2+CD133+ cells. Images were taken at 100× magnification. Bar, 100 μm.

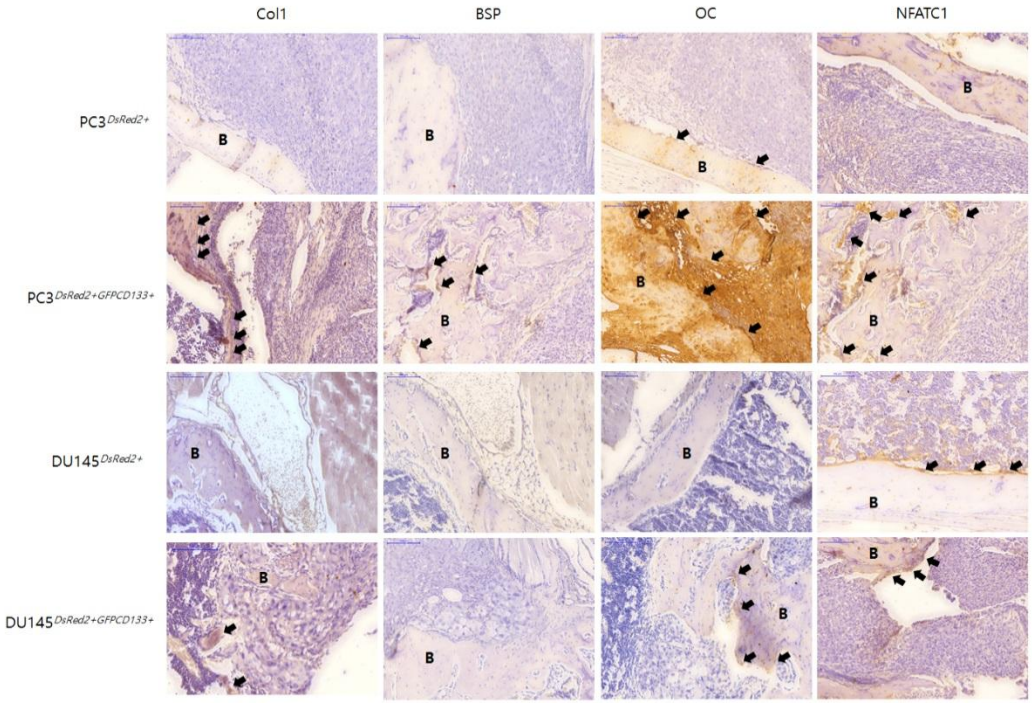

Figure 13. Immunohistochemical analysis of Col 1, BSP, OC, and NFATC1 expression in intra-tibial tumors formed by PC3DsRed2+/PC3DsRed2+CD133+ or DU145DsRed2+/DU145DsRed2+CD133+ cells. Negative controls were incubated without the primary antibody. Black arrows denote areas of high expression. Images were taken at 200× magnification. Bar, 100 μm.

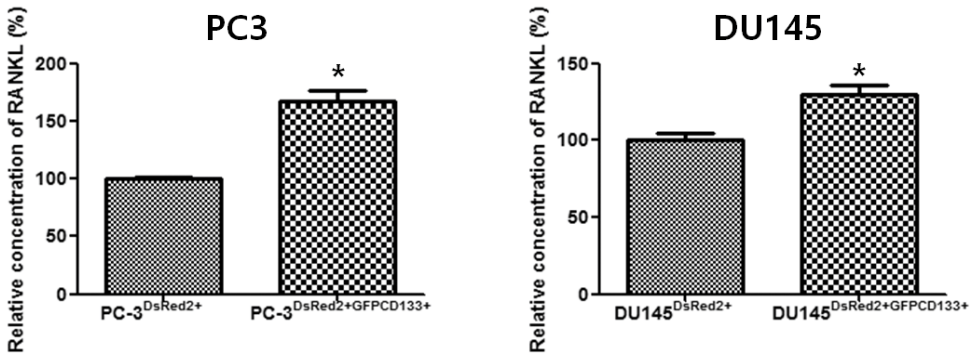

Figure 14. Concentration of RANKL in cell culture supernatants. Data in the bar graphs are expressed as the mean ± standard deviation.

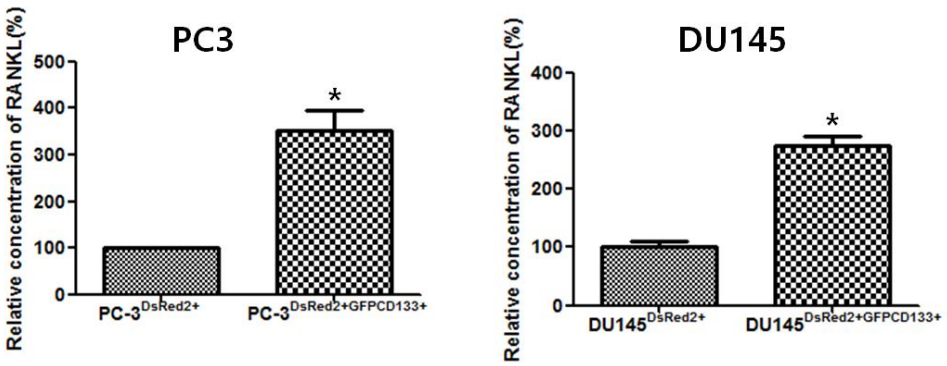

Figure 15. Concentration of RANKL in serum from tumor-bearing mice. Data in the bar graphs are expressed as the mean ± standard deviation.